Gaseous and Particulate Emissions with Jet Engine Exhaust and Atmospheric Pollution

A.M. Starik
Central Institute of Aviation Motors
Aviamotornaya St., 2, Moscow, 111116, Russia

e-mail: star@ciam.ru

ABSTRACT

The features of nonequilibrium processes in combustor, postcombustor flow, and in the plume of gas-turbine engines which are responsible for the formation of gaseous pollutants, mainly, SO_x, NO_x, CO_x, HO_x, HSO_y, HNO_y, and ions as well as for processes that give rise various sorts of volatile and nonvolatile (with soot core) aerosols and ice particles are considered. The results of numerical simulation as well as experimental studies of these processes are reported.

Key words: nonequilibrium physico-chemical processes, combustor, plume, pollutants, ions, aerosols, atmosphere.

INTRODUCTION

The aviation is the source of gaseous and particulate emissions into the atmosphere. The number of species emitted by jet engine is much enough and depends on a kind of a fuel and on an engine design. The emission from aviation engines is significantly smaller (in a factor of 40-50) than that from surface sources. However, because the emissions of aircraft engines occur in the atmospheric regions (high troposphere and low stratosphere), which are very sensible to various perturbations, the problem of aviation effect on atmospheric processes and climate change has come into great importance [1].

The impact of aviation on the atmosphere is under way through the complex of interconnected processes. In present, there are no any standard limitations for the concentrations of gaseous and particulate pollutants emitted by aircraft engines at cruise altitudes. Nevertheless, it is believed that emissions of different gaseous species and aerosols by aviation engines are of reverence to the impact of aviation on atmospheric chemistry, ozone depletion, and climate [1-3]. Numerous model investigations showed that gaseous species, mainly NO_x, HO_x, CO_x, SO_x, organics, emitted from aircraft engine as well as combustion and newly formed in the exhaust plume aerosols may influence significantly the total ozone concentration, cloudiness, Earth's radiation budget, and climate.

The ozone layer is a term that refers to the distribution of ozone that is naturally formed in the stratosphere. This layer protects life on Earth from harmful levels of solar ultraviolet radiation. Climate is defined as the typical behavior of the atmosphere, the aggregation of the weather, and is generally expressed in terms of averages and variances of temperature, precipitation and other physical properties. Climate is being affected by human activities that emit radiatively active substance such as greenhouse gases or aerosol particles. Greenhouse gases in the atmosphere absorb infrared radiation, especially in the "atmospheric window" region from 8 to 12 μm, that would otherwise escape to space. This trapped radiation warms the atmosphere, creating a positive radiative forcing which in turn warms the Earth's

Starik, A.M. (2008) Gaseous and Particulate Emissions with Jet Engine Exhaust and Atmospheric Pollution. In *Advances on Propulsion Technology for High-Speed Aircraft* (pp. 15-1 – 15-22). Educational Notes RTO-EN-AVT-150, Paper 15. Neuilly-sur-Seine, France: RTO. Available from: http://www.rto.nato.int.

surface. Aerosols, on the other hand, scatter or absorb solar radiation and prevent it from reaching the Earth. This has a net cooling effect. Together, emissions of greenhouse gases and aerosols destroy the existing radiative balance of the atmosphere and alter the heating and cooling rate of the Earth.

In view of the aviation impact on the atmosphere, the following gaseous species can play the most important role: NO_x ($NO+NO_2$), HNO_y (HNO_2+HNO_3), SO_x (SO_2, SO_3), H_2SO_4, HO_x (OH, HO_2, H_2O), CO_x (CO, CO_2), and nonmethane hydrocarbons. The elements of NO_x and HO_x groups participate in the catalytic cycles of ozone destruction and the abundance of the species HNO_2, HNO_3, and NO_2 as well as H_2O can results in a broadening of the polar stratospheric cloud formation areas due to appearance of additional HNO_3 and H_2O in Polar Regions. The element of CO_x group (especially CO_2) and hydrocarbons are greenhouse gases and affect the Earth's radiative balance.

Besides the gaseous species, aircraft engines emit aerosol particles and aerosol precursors. Soot and metal particles are directly emitted by aircraft engines. Soot particles are believed to be the most important aviation aerosols impacting contrail and cirrus cloud formation. As Lohmann and Feichter pointed out in a recent review of the global indirect aerosol effects [3], black carbon, which is a major constituent of carbonaceous particles emitted from incomplete combustion processes, contributes to the direct aerosol radiative effect by absorption of visible radiation which results in a net reduction in shortwave radiation and thus a negative forcing at the surface [3]. At the top-of atmosphere, carbonaceous particles exert a positive forcing. This effect can be amplified if absorption of solar radiation by carbonaceous particles occurs within cloud droplets. Since aerosol particles are predominantly a complex internal mixture of chemical substances, the effects of coating insoluble black carbon particles with soluble organic or inorganic species may have a strong effect on the cloud condensation nuclear (CCN) activation of those particles. The knowledge of the coating effects is in turn a prerequisite for an adequate treatment of carbonaceous particles in global climate models.

The newly formed in the exhaust plume aerosols are mainly the sulfate volatile aerosol particles. The formation of sulfate (H_2O/H_2SO_4) liquid small droplets (diameter of 1-10 nm) in generally caused by emission of condensable gases such as water vapor (H_2O) and gaseous H_2SO_4 or SO_2 and SO_3 which can be converted to H_2SO_4. Besides oxidized sulfur in different forms (SO_x, H_2SO_4) and water vapor, aerosol precursors emitted by aviation engine include chemi-ions, HNO_3, and unburned hydrocarbons (organics). A number of modeling studies have demonstrated that the emission of sulfur oxides (SO_2, SO_3) and, especially, of sulfate aerosol particles can considerably affect the surface area of the sulfate stratospheric aerosol layer. Moreover, the emission of sulfate aerosol particles into the stratosphere caused by the fleet of supersonic high-speed civil transport aircraft, known as HSCTs, can result in ozone depletion.

In order to obtain the required information about pollutants emitted by aircraft engines it is needed to conduct the investigations on the following topics: (1) formation of SO_x, HSO_y, NO_x, HNO_y, HO_x, $C_xH_yO_z$ species, ions, and soot particles during the burning of high-order hydrocarbons (aviation kerosene) with air in aero-engine combustor; (2) evolution of gaseous and particulate species (soot particles) in the postcombustor flow of jet engine; (3) generation of ionic clusters and binary H_2O/H_2SO_4 (or ternary $H_2O/H_2SO_4/HNO_3$, H_2O/H_2SO_4/organics) volatile aerosols in aircraft plume, formation of the coverage onto soot particle surface, and condensation of water vapour on activated large soot particles; (4) freezing of soluble material accumulated on the surface of soot particles and contrail formation.

The general objective of this paper is to discuss the nonequilibrium processes in the combustor and in the postcombustor flow of gas-turbine engine that are responsible for gaseous pollutant formation and processes that give rise various sorts of volatile and non-volatile (with soot core) aerosols and ice particles in the plume.

FORMATION OF GASEOUS SPECIES, CHEMI-IONS, AND SOOT PRECURSORS IN AVIATION COMBUSTOR

In present, for commercial aircraft engines the aviation kerosene is used as a fuel. Aviation fuels are comprised of numerous hydrocarbons such as n-parafins, iso-paraffin, naphtene (cycloparaffin), aromatics, alkenes, and sulfur in a trace amount [4]. Table 1 lists the properties and average composition of the typical aviation fuels. Different surrogate blends have been proposed to model the ignition/combustion of aviation fuels [4]. For example the possible JP-8 surrogate consists of 5% iso-octane, 5% methyl cyclohexane, 5% m-xylene, 5% cyclooctane, 15% butyl benzene, 15% tetradecane, 10% hexadecane, 5% butyl benzene, 5% tetralin, 5% l-methyl naptalen, and 5% 1, 2, 4, 5-tetramethyl benzene. The complexity associated with the chemical composition of kerosene-type fuels is well recognized [5], and a detailed computational consideration of all of the fuel components of kerosene would be prohibitive. Doute et al. [6] report a chemical analysis of 79-mol % alkanes, 10-mol % cycloalkanes, and 11-mol % aromatics for the fuel utilized in their investigation of kerosene flames. As was shown in [5] the chemical structure of n-decane and kerosene flames is marked similarities. Thus the chemical composition of kerosene may be modeled by a surrogate blend comprising 89-mol % n-decane and 11-mol % aromatic fuel, example, benzene, toluene, ethyl benzene, and naphthalene.

Table 1. Typical aviation fuel properties

Property	JP-4	JP-5	JP-7	JP-8 (Jet A/A-1)	RP-1
Approx. formula	$C_{8.5}H_{17}$	$C_{12}H_{22}$	$C_{12}H_{25}$	$C_{11}H_{21}$	$C_{12}H_{24}$
H/C ratio	1.99	1.87	2.02	1.91	1.98
Boiling range	140-460	360-495	370-480	330-510	350-525
Freeze point	-80	-57	-47	-60 JP-8/Jet A-1; -50 Jet A	-55
Avg. composition					
Aromatics, vol %	10	19	3	18	3
Naphthenes	29	34	32	20	58
Paraffins	59	45	65	60	39
Olefins	2	2	—	2	—
Sulfur, ppm	370	470	60	490	20

The kinetic model for kerosene surrogate blend should be supplemented by reaction mechanisms of S- and N-containing species and chemi-ions (CIs) formation. Aviation kerosene contains between 0.001% and 0.3% sulfur per mass. Sulfur is present in the fuel as a compound of aromatic groups of hydrocarbons. During the oxidation, the various S-containing species (in the fuel lean flame, mostly SO_x (x=1, 2, 3) and HSO_3) forms. The kinetic model should describe rather accurately the proportions between SO_2, SO_3, and HSO_3. Such a model was developed by Starik et al. [7]. The point is that the most particles forming in the exhaust plume behind aircraft at cruise are liquid and contain sulfuric acid [8], and some condensable hydrocarbons [9]. The formation of volatile aerosols in the aircraft plume depends on the concentration of gaseous O, OH, SO_2, SO_3, H_2SO_4, and on CIs emitted by the engine. The concentrations of OH, SO_3, and H_2SO_4 at core engine exit depend on the non-equilibrium chemistry in the combustor and in the postcombustor flow from the combustor through the turbine and the expansion nozzle to the engine exit [10, 11].

N-containing species are generated due to oxidation of air nitrogen in the high temperature region inside a combustor. The main species formed in an aviation combustor are NO and NO_2. The following mechanisms is believed to be responsible for NO_x production: (1) extended Zel'dovich mechanism; (2) "promt NO" or Fenimor mechanism; (3) NO_2 mechanism; (4) N_2O mechanism; (5) NNH mechanism. The extended Zel'dovich mechanism involves the oxidation of N_2 by O_2: $N_2+O=NO+N$, $N+O_2=NO+O$ and reaction of N atoms with OH radicals $N+OH=NO+H$. The Fenimor mechanism passes via HCN: $CH+N_2=HCN+N$, $O+HCN=NO+CH$ and occurs, mostly, in a fuel rich flame. The N_2O mechanism is the summation of NO production in the course of reactions with N_2O: $N_2O+CO=NCO+NO$, $N_2O+H=NH+NO$, $N_2O+O=2NO$. The NO_2 mechanism specifies the NO production in the course reactions with NO_2: $NO_2+CO=NCO+NO$, $NO_2+OH=HO_2+NO$, $NO_2+H=OH+NO$, $NO_2+O=NO+O_2$, $NO_2+M=NO+O+M$. The NNH mechanism involves the reactions with HNO and N_xH_y species.

Besides the NO and NO_2 formation, the kinetic mechanism of N-containing species production should describe also the formation of N_2O, HNO, HNO_2, HNO_3, NO_3, N_xH_y, proportions between NO and NO_2 and between NO_x ($NO+NO_2$) and NO_y ($NO_y=NO_x+N_2O+NO_3+HNO_y$). The ratio of NO_2 to NO_x concentration was measured in the exhaust plume for several aviation engines and varies from 5% to 25% [12]. The NO_y/NO_x concentration ratio is close to 0.01 [13]. The quantitative information about HNO_2 and HNO_3 emissions from aircraft is extremely important for atmospheric chemistry, formation of polar stratospheric clouds, and prediction of the aviation effect on the atmosphere. For the aviation combustor operating in a diffusion mode, the Zeldovich and Fenimor mechanisms are mainly responsible for NO formation. Also the NO_2 mechanism plays a noticeable role in the NO_x production inside the combustor. It is worth noting that NO and NO_2 production inside the aviation combustor are in a strong interconnection. The N_2O and NNH mechanisms give smaller contribution in NO formation [14].

In order to predict the emissions of NO_x, CO_x, and unburned hydrocarbon (UHC) the two different approaches has been developed. One of them is based on semi-empirical formulas so-called correlation models that include the pressure and temperature of the gas at the combustor inlet as well as the residence time for the gas inside the combustor (see, for example [15]). The other one is based on the use of multi-reactor models, which calculate the concentrations of NO_x, CO_x, HO_x, UHC, and the other species in the each individual reactor by using the detailed kinetic reaction mechanism [14]. Note that this approach may be used also to predict the emissions of S-containing species and CIs. To construct the reactor model, the information on fields of the temperature and other flow parameters inside the combustor is required. To obtain these fields the three-dimensional (3D) numerical simulation of turbulent combustion using the CFD code with the equilibrium chemical model may be applied. Fig.1 shows the temperature field inside the typical aviation combustor (this combustor is similar to that for PC-90A turbo-jet engine) computed using standard STAR-CD software [14].

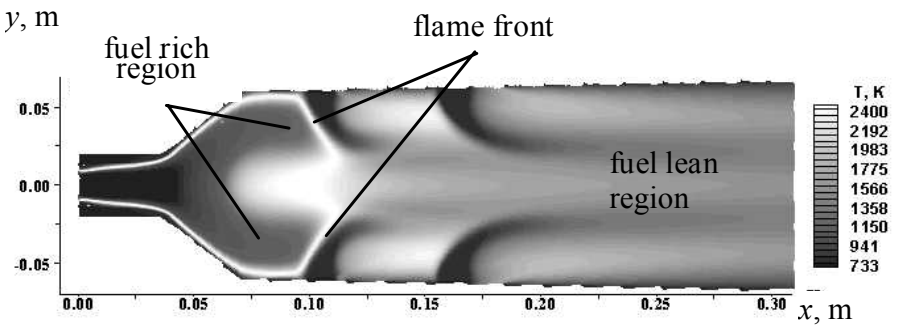

Fig. 1. The temperature field inside the conventional aviation combustor.

The simulations have demonstrated that predicted NO_x emission index strongly depends on the applied kinetic reaction mechanism. This illustrated by the data on the measured and computed using the different kinetic models [16-18] the NO_x emission index $EINO_x$ ($EINO_x = G_{NO_2} / G_f$, where G_{NO_x}, G_f are the mass flow rates of NO_x and fuel, respectively) for typical aviation combustor operating in a diffusion mode (gas residence time of 6.7 msec, the pressure of 10^6 Pa) for two values of the temperature at the combustor inlet T_{air}=600 and 660 K presented in Fig.2. One can see that only the prediction using the DS reaction mechanism is consistent with experimental data. The widely applied GRI-Mech 3.0 and Konnov 0.4 reaction mechanisms underestimate the NO_x emission considerably. Furthermore, the GRI-Mech 3.0 and Konnov mechanisms underestimate the NO_2/NO_x ratio (the predicted value of this ratio is as small as 1%). The DS reaction mechanism predicts the NO_2/NO_x ratio of 5-10% that is consistent satisfactorily with experimental data.

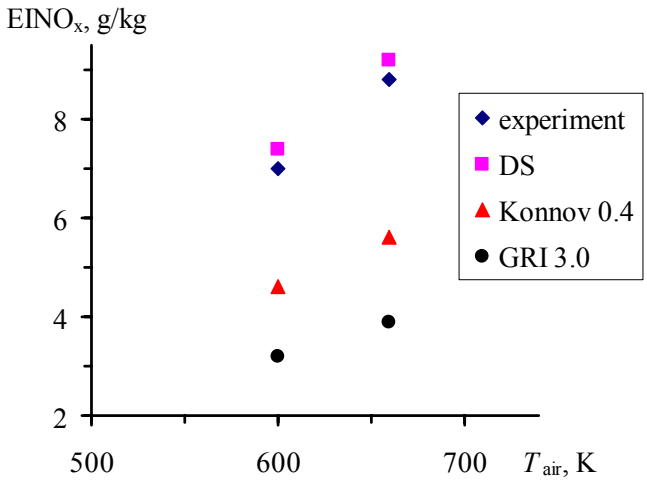

Fig. 2. Measured and predicted using different kinetic mechanisms (GRI 3.0, [16], Konnov 0.4 [17], and DS [18]) NO_x emission index, $EINO_x$, as a function of the combustor inlet temperature.

For modern gas-turbine engines the values of $EINO_x$ vary from 12 to 40 g/kg fuel. In order to lower significantly the NO_x emission up to $EINO_x$=5-8 g/kg the lean premixed and prevoparised (LPP) technology has been proposed. In LPP combustor a homogeneous burning of lean fuel/air mixture (equivalence ratio 0.6-0.5) takes place. In this case, the maximal temperature inside the combustor does not exceed 2100 K that is significantly smaller than that for traditional diffusion combustor (T=2400 K). This reduces the rate of NO_x production in the course of Zeldovich mechanism. However, the LPP combustor exhibits the worse re-light and blow-out characteristics as compared to conventional diffusion combustor.

Besides SO_x and NO_x species, the CO, CO_2 and unburned hydrocarbons (C_xH_y) form inside the combustor. The emission indices for various species depends on the engine power setting. The computations carried out by using the multi-reactor model [14] exhibited that the decrease in power setting results in a strong increase of EICO and EIC_xH_y and, conversely, in decrease of NO_x and CO_2 emissions. The value of $EISO_2$ does not depend markedly on power setting. Table 2 lists the predicted emission indices for NO_x, CO, C_xH_y, SO_2, SO_3, species, as well as the values of residence time pressure and temperature of the air at the combustor inlet for different power settings at FSC=0.04%.

Table 2.

Parameters / Power setting	P, MPa	T_{air}, K	$EINO_x$, g/kg	EICO, g/kg	EIC_xH_y, g/kg	$EISO_2$, g/kg	$EISO_3$, g/kg
100% τ_{res} = 13.63 ms	2.14	755	36.4	0.72	0.06	0.783	0.0199
85% τ_{res} = 13.78 ms	1.88	727	29.2	11.3	1.2	0.781	0.0213
30% τ_{res} = 14.78 ms	0.89	591	12	76.7	12.9	0.748	0.0256
7% τ = 17.14 ms	0.41	485	8.7	105	18.8	0.723	0.0205

The important precursors of volatile aerosol particles are CIs, which form in the combustor during the combustion of hydrocarbon fuel with air via radical-radical and ion-molecular reactions [7, 19]. CIs may induce the nucleation of volatile aerosols and promote the growth of aerosols via ion-assisted coagulation [20]. Another possible mechanism of CIs influence on volatile and nonvolatile (with soot core) particle formation is connected with ion-soot interaction. CIs may attach to soot particles, induce the charge, and as a consequence enhance the water uptake by soot particles [21].

It should be noted that the most studies on ion formation were conducted for flames [19]. Ion composition strongly depends on the fuel/air equivalence ratio, ϕ, and on the type of fuel (hydrogen, hydrocarbons, aviation kerosene, etc.). The most frequently used technique to measure an ion concentration in flame is massspectrometry [19]. Numerous types of positive and negative ions such as $C_2H_3O^+$, $C_3H_3^+$, CH_3^+, HCO^+, $C_3H_5O^+$, $C_3H_7O^+$, H_3O^+, H_2O^+, O_2^+, NO^+, NO_2^+, HCO_2^-, HCO_3^-, CO_3^-, CO_4^-, O_2^-, OH^-, NO_2^-, NO_3^-, CN^- were observed in hydrocarbon/air flames. In fuel rich flames, heavy hydrocarbon ions $C_{13}H_9^+$, $C_{19}H_{11}^+$, $C_{22}H_{12}^+$, $C_{55}H_{19}^+$, as well as positively charged fullerene molecules may form [22]. Measurements behind the aviation combustor demonstrated the presence of $C_xH_yO^+$ and $C_xH_yO^-$ ions as well as SO_3^-, SO_4^-, and HSO_4^- ions [23]. In order to understand the mechanisms and principal pathways of ion formation the experimental data should be supplemented by numerical simulation. In this light, rather complicated kinetic models for charged species formation during combustion of various fuels have been developed [7, 24].

The processes of ion formation inside the aero-engine combustors are more complicated than those in flames. The modern combustor operates in a diffusion mode. In this case, the fuel/air mixture composition differs considerably in various regions of combustor. Therefore, a number of different ions can form inside the combustor. The gas residence time for combustor (5-10 ms) is much smaller than that for flame (~100 ms). The total ion concentration of $\sim 2 \cdot 10^8$ cm^{-3} at the exit plane of aero-engine combustor was measured recently by Haverkamp et al. [25]. However, inside the combustor, the concentration of ions and electrons may be estimated only by computations. To simulate the processes of charged gaseous species formation inside an aviation combustor one have to apply approximate combustion models, for example, Flame Let model [26]. In our computations this model was supplemented by the ion kinetics developed in [7, 24]. To calculate the flow parameters inside the combustor (these parameters are needed as input ones for the Flame Let model) with outlet pressure of 10^6 Pa and temperature T_c = 1540 K the 3D numerical simulation of turbulent combustion using the standard STAR-CD software with the equilibrium chemistry was conducted [27].

Inside the combustor the maximal concentration for the most abundant ions in flames, $C_2H_3O^+$, is observed in the fuel rich region located ahead of the flame front (see Fig. 1) and attains $10^{11} - 10^{12}$ cm^{-3}. In this region, the maximal concentration for negatively charged species is appeared for electrons and HCO_2^- ions. However, at the combustor exit the concentrations of these species are negligible. In the fuel lean zone of combustor at the exit section only NO^+, H_3O^+, SO_3^-, HSO_4^- or $NO_3^- NO^-_3$ ions remain to be abundant. The predicted total concentration of positive (negative) ions in the combustor outlet is around $2 \cdot 10^8$ cm^{-3} [27] that is in a good agreement with measurements [25]. It is worse noting that the ion composition strongly depends on the value of fuel sulphur content (FSC). The principal scheme of ion formation in hydrocarbon flames and inside the combustor is presented in Fig.3.

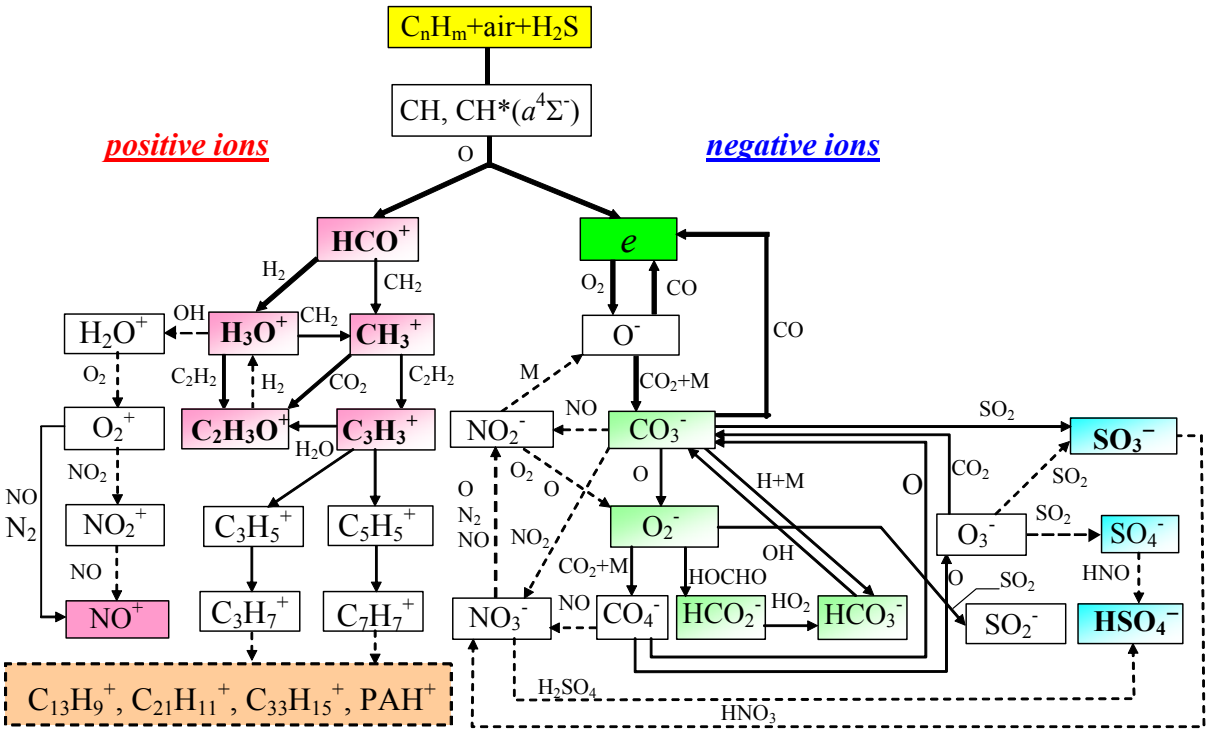

Fig. 3. Principal scheme of ion formation in hydrocarbon+air flame.

Soot particles form in the fuel rich zone of combustor due to clustering and heterogeneous surface growth of primary soot precursors such as polyyne molecules, and polyaromatic hydrocarbons [28]. In accordance to modern models, the pyrene molecules which consist of four aromatic rings are the main soot precursors. The particle inception with radius of approximately 1 nm is constructed from PAH. In the fuel rich zone of combustor the concentration of pyrene molecules can be as large as $10^{12} - 10^{14}$ cm^{-3} and concentration of primary clusters (particle inception) attains $10^{11} - 10^{12}$ cm^{-3}. It should be noted that combustion exhausts are the typical dusty plasma. It consists of various molecular gases, ions, electrons, carbon clusters, and soot particles. Therefore, in order to predict the charge and size distribution of soot particles it is needed to take into account the plasma-chemical processes occurring inside the combustor. Figure 4 shows the principal scheme of soot particle formation.

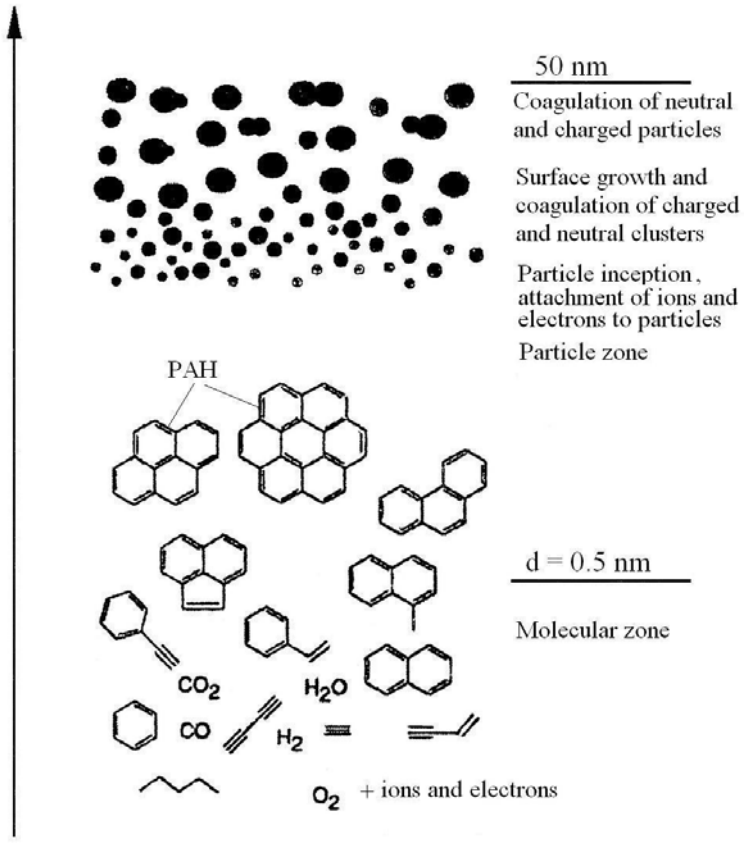

Figure 4. A rough picture for soot formation in combustion plasmas.

Ions and electrons originated in the fuel rich zone of combustor attach to small clusters and soot particles. As a result primary neutral clusters and particles acquire a significant charge [21]. Charged clusters with opposite polarities coagulate more rapidly than neutral ones. The charged cluster induces the image charge on a neutral particle. Therefore, for charge-neutral cluster (particle) interaction the appearance of the image force enhances the cluster coagulation [29] and, as a consequence, facilitates the formation of soot particles [30]. Fig. 5 depicts the predicted charge distribution of clusters with different sizes formed from the neutral monodisperse primary precursors of initial concentration $N_0=10^{11}$ cm^{-3} with radius $a_0=1$ nm at time instants t = 0.1 and 5 ms. One can observe that at an initial stage even small size clusters are principally charged negatively due to the strong electron attachment. At the latter time instant the charge distribution becomes to be more symmetrical and the size of clusters increases. Even small clusters with radius a = 4 nm may acquire the charge Q=4-5e (e is an elementary charge). Larger size soot particles with $a \approx 40$ nm acquire the charge of (15-30)e in the region placed directly ahead of the flame front [21].

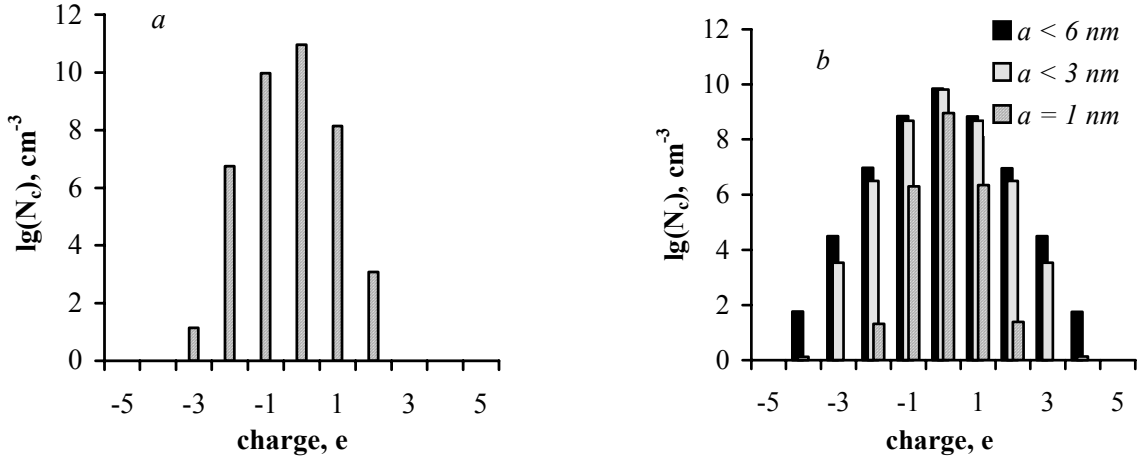

Figure 5. Predicted charge distribution of clusters with radii smaller than given value at N_0=10^{11} cm^{-3} and a_0=1 nm at the conditions in the fuel rich region of combustor for time instants of 0.1 ms (*a*) and 5 ms (*b*).

The existence of a charge on the cluster (or soot particle) surface enhances the uptake of the molecules having a permanent dipole momentum by cluster and soot particle. For example, the attachment coefficient for H_2O molecules to the cluster with a = 4 nm and Q=5e is by a factor of 10 larger at T=2000 K, P=10^6 Pa than that for neutral cluster. Calculations showed that a noticeable proportion of soot particles (~10%) having a relatively large charge can accumulate the water soluble compounds inside a combustor. Thus, this fraction of soot particles may be activated to act as contrail nuclei with in an engine.

The analysis of the IR-Fourier spectra of combustor-generated soot particles exhibited that combustor soot consists of two different fractions: a main fraction containing, mostly, amorphous carbon and a fraction of impurities specified by a complex structure and a noticeable amount of water soluble compounds such as organic sulfates, S-containing ions, and organic molecules on the surface of soot particles. It was observed that ~13.5 wt % of water soluble fraction may be appeared on the soot particles within a combustor [30, 31]. The main fraction is supposed to form from neutral clusters or particles with a small charge, $Q \leq 2e$. These particles can not accumulate polar molecules within a combustor and are hydrophobic. Conversely, the fraction of impurities demonstrates the high level of hydrophilicity [30, 31].

NONEQUILIBRIUM PROCESSES IN TURBINE AND NOZZLE FLOW

Rapid expansion of hot gases with a complex composition through the turbine and nozzle (the residence time is ~5-7 ms) causes the nonequilibrium chemical transformation and ion-soot attachment due to change of temperature and pressure [10, 11, 32]. The typical values of temperature at combustor exit for modern engines are ~1300-1800 K and at the nozzle exit ~450-650 K. The pressure in these sections for cruise regime varies in the range 0.8-1.2 MPa and in the range 10-20 kPa, respectively.

In present, to investigate the nonequilibrium processes in the postcombustor flow of jet engines the numerical simulation is used. The computation of the evolution of the chemical composition of combustor exhaust gases in the turbine and nozzle flow for modern aero-engine at cruise of *B-747* aircraft (Mach number M_0=0.8 and altitude H=10.8 km) based on the quasi-one dimensional (Q1D) model [7] showed that the mole fractions, γ_i, vary considerably for most of the mixture components with minor variations only for H_2O, O_2, N_2, and CO_2. The variations of the γ_i values are most pronounced for strong oxidizers such as O, OH, and HO_2, as well as for NO_3 and for the species of the N_xH_y group. The effective mass emission index of OH amounts to 5.4 g/kg at combustor exit and 66 mg/kg at engine exit. At engine exit,

most of the initially formed OH radicals are depleted by reactions with NO, NO_2, SO_2 and others, leaving a mole fraction of about 10^{-6}, and this explains why measurements so far found hardly significant traces of OH at engine exit [33]. From measurements of HNO_2, HNO_3, NO, and NO_2 in aged exhaust plumes, OH emission indices of 60 to 400 mg/kg have been derived using models describing the chemistry in the diluting plume, starting from engine exit [34]. This fits reasonably with the present model results. The small amount of OH emitted from the engine exit implies small (<1%) additional sulfur conversion to H_2SO_4 after engine exit. It should be noted that the concentrations of HNO_2 and HNO_3 in the turbine affect each other.

Significant SO_2 oxidation occurs throughout the turbine and nozzle resulting in up to 10% oxidation of the total SO_x to (SO_3+H_2SO_4) at the engine exit. The NO_3 and HNO_2 concentrations also increase significantly within the postcombustor flow but stay below 1% of the sum of NO and NO_2 species, as found in measurements [34]. Concentrations of sulfur species SO_2, SO_3, and H_2SO_4 at the engine exit strongly depend on FSC. Note that even for FSC=0 the marked amount of gaseous H_2SO_4 and HSO_4^- ions may be abundant in the nozzle exhaust. This is caused by the presence of S-containing species, mainly COS, H_2S, SO_2, in the atmospheric air, which is supplied to the combustor. For FSC=0 the concentration of the gaseous H_2SO_4 achieves $2.5\cdot10^8$ cm^{-3}. The abundance of gaseous H_2SO_4 in the engine exhaust at FSC=0% leads to formation of small sulfate volatile particles (with diameter $d \leq 1$ nm) in the plume (see below). During expansion of combustion exhausts throughout the turbine and nozzle, the concentrations of different gaseous species may vary significantly. This is clearly seen from the data presented in Table 3.

Table 3. Predicted species molar fractions at the different sections of the modern gas-turbine engine at FSC=0.04 %

Parameters and species	Combustor	Turbine	Bypass flow	Mixer	Nozzle
T, K	1414	774	375	480	473
P, kPa	2080	167	101	167	166
O_2	1.26(-1)	1.26(-1)	2.00(-1)	1.82(-1)	1.82(-1)
H_2O	4.96(-2)	4.96(-2)	5.77(-5)	1.25(-2)	1.25(-2)
SO_2	7.68(-6)	7.33(-6)	3.79(-9)	1.83(-6)	1.84(-6)
SO_3	1.56(-7)	4.89(-7)	0	1.22(-7)	3.99(-8)
H_2SO_4	4.36(-11)	2.47(-8)	5.06(-13)	6.20(-9)	8.89(-8)
N_2	7.79(-1)	7.79(-1)	8.00(-1)	7.94(-1)	7.94(-1)
NO	4.80(-4)	4.78(-4)	1.00(-11)	1.20(-4)	1.20(-4)
NO_2	1.68(-5)	1.66(-5)	6.03(-12)	4.18(-6)	4.22(-6)
HNO_2	9.65(-8)	2.39(-6)	0	5.99(-7)	6.01(-7)
CO	1.61(-5)	1.28(-5)	2.28(-7)	3.38(-6)	3.38(-6)
CO_2	4.44(-2)	4.44(-2)	3.09(-4)	1.13(-2)	1.13(-2)

Decrease of FSC value results in the change of ion composition both at the combustor and at the nozzle exit. The concentration of ions grows with the FSC increase. The total number density of positive (negative) ions at the engine exit may vary in the range $2\cdot10^7 - 2\cdot10^8$ cm^{-3}. For the free sulfur fuel the concentration of NO_3^- and NO_2^- ions becomes noticeable and is comparable with the concentration of HSO_4^- ions.

During expansion through the turbine and nozzle, soot particles may change their charge as a result of continuous charging and discharging events in a bipolar ion environment. To simulate the processes of the soot particles charging in the turbine and nozzle flow the Q1D code with coupled gas phase ion and neutral species kinetics, and kinetics of accumulation of a charge on soot particles with different radii was

developed [32]. The computations performed for cruise regime of *B-747* aircraft showed that ion-soot interaction in the postcombustor flow leads to evolution of soot particles charge just in the high pressure turbine of the engine.

At the nozzle exit the rather small soot particles with $a \leq 10$ nm may accumulate only two elementary charges. Large particles with $a \approx 60$ nm may accumulate the elementary charges of 4-5. Due to smaller mass of positive ions (NO^+, H_3O^+) as compared with that for negative ions (HSO_4^-, NO_3^-), which are abundant at combustor exit, the concentration of positively charged soot particles are larger than negatively charged ones. The proportions of neutral, positively and negatively charged soot particles depend on the fraction of charged soot particles in combustion products. The predicted charge distribution of soot particles (the median radius of lognormal size distribution is 25 nm, and geometrical deviation is 1.57), $N_s(a)$, at the nozzle exit of *RB-211* engine at *B-747* aircraft cruise regime of are presented in Fig. 6.

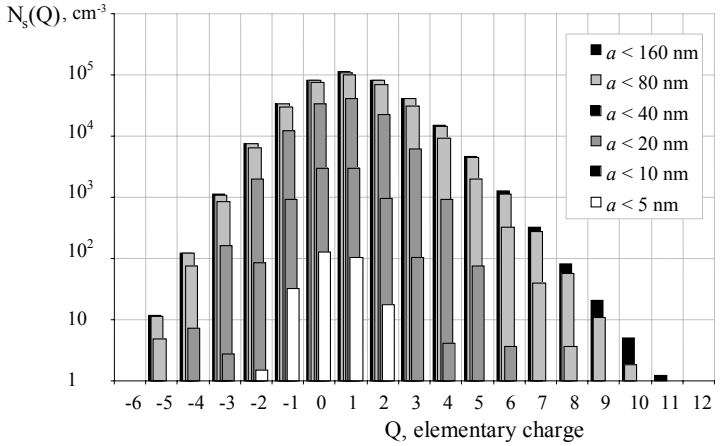

Fig. 6. Predicted charge distribution of soot particles with different radii, *a*, and total concentration N_s^0 =8·10^6 cm^{-3} at the nozzle exit of *RB-211* engine at cruise regime of *B-747* (M_0=0.8, *H*=10.8 km).

FORMATION OF AEROSOL PARTICLES IN AIRCRAFT PLUME

There are a number of gaseous pollutants, ions, aerosol precursors, charged and neutral soot particles in the engine exhaust. Cooling of hot exhaust gases ($T \approx 600$ K) caused by mixing with co-flow atmospheric air (T_a=200-220 K) leads to an occurrence of a complex of nonequilibrium processes resulting in transformation of chemical composition of exhaust gases, formation of ionic clusters, mostly, $HSO_4^-(H_2SO_4)_n$ (n=1…3), $NO_3^-(HNO_3)_n(H_2O)$, $HSO_4^-(HNO_3)_n$, $HSO_4^-(SO_3)$, $H_3O^+(H_2O)_m$, $H_3O^+(CH_2O)(H_2O)_m$, m=1..9, generation of liquid volatile H_2O/H_2SO_4 small aerosol particles with diameter d≤10 nm, production of large particles with soot core coated by liquid soluble materials or by freezed solution [35-38]. The size of soot particles and ice particles are in the range 10 nm – 1 μm. Fig. 7 shows the size distribution of volatile (d≤10 nm) and non-volatile particles in the plume of ATTAS aircraft [35]. The microphisical processes which are responsible for volatile and non-volatile aerosol particle formation in the aircraft plume are rather complicated. The schematic of these processes are presented in Fig. 8.

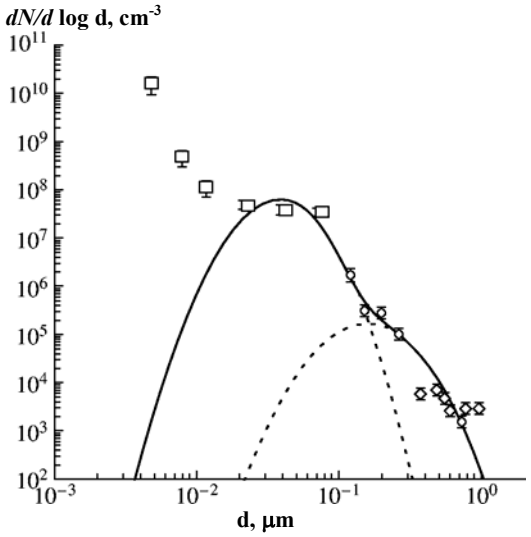

Fig. 7. Size distribution of aerosol particles (d is the particle diameter) in the plume of ATTAS aircraft. Dashed, dotted, and solid lines correspond to the mode of primary soot particles, mode of agglomerated particles, and total distribution of soot particles. Measurements: squares, rhombuses, and circles.

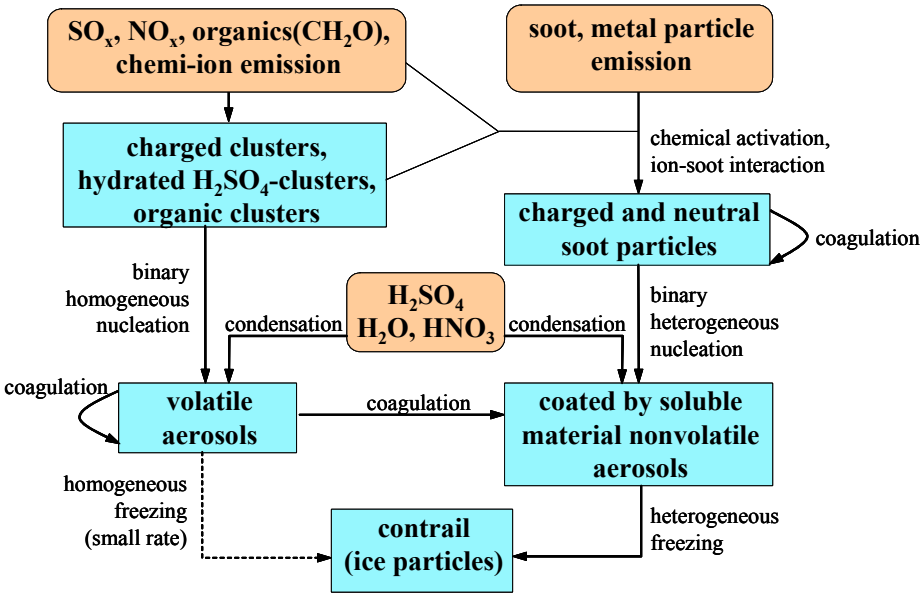

Fig. 8. The schematic of processes being responsible for aerosol particle formation

Despite of a number of experimental and numerical investigations of the microphysical processes in the plume many questions are still unresolved. Up to now there is lack of quantitative consistent between computed and observed data on volatile aerosols particle concentration in the plume. Moreover, the main mechanisms of formation of relatively large volatile particles with d>5 nm are not still undetermined. Two hypotheses were proposed to improve the agreement between simulation and in-situ measurements of number density of large-size volatile aerosols. First, it was hypothesised that abundance of SO_3 additionally to SO_2 at the nozzle exit results in a growth of the size and number density of volatile aerosol particles [40]. Previous analysis prescribed the SO_3 concentration at the nozzle exit as a free model

parameter and did not take into account the presence of HSO_3 and H_2SO_4 species at the nozzle exit besides SO_3. However, as it was shown above these species may be abundant at the nozzle exit as a result of a strong oxidation of SO_2 and SO_3 in the turbine and nozzle flow.

As compared to the case where only SO_2 is abundant at the nozzle exit, the analysis demonstrated that the presence of SO_3, HSO_3, and H_2SO_4 species in the nozzle exhaust leads to an increase of H_2SO_4 partial pressure, nucleation rate, sulfur conversion efficiency, intensification of coagulation processes, change of the particle size distribution, and an increase of the number of large-size volatile aerosols in the near field plume. Fig. 9 depicts the evolution of the H_2O/H_2SO_4 volatile aerosol number density, N_a, with different diameters along *B-747* aircraft plume axis at cruise for FSC=0 % and 0.04 % when all S-containing species are present in the nozzle exhaust and when only SO_2 is abundant at the nozzle exit. Markedly, that even for FSC=0% the abundance of SO_3 and H_2SO_4 which are produced in a combustor due to burning the hydrocarbon fuel with atmospheric air containing sulfur species, results in a formation of sulfate aerosols in the plume (at 100 m – 150 m distance from nozzle exit). But diameter of these volatile particles does not exceed 1.2 nm and concentration of the particles with d > 1 nm is around 10^4 cm^{-3}. When only SO_2 is abundant at the engine exit there are no any sulfate aerosols in the plume [38].

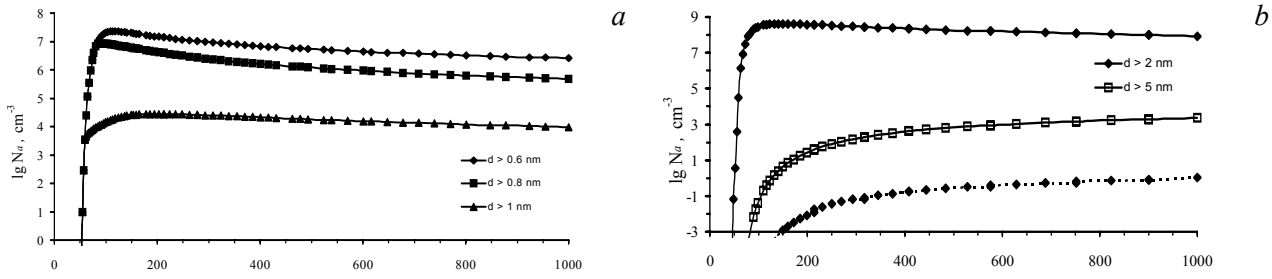

Fig. 9. Predicted evolution of the number density of volatile H_2O/H_2SO_4 aerosol particles with particle diameters larger than a given size d along the plume axis of *B-747* for two cases of initial S-containing species abundance at the engine exit: all S-containing species are present (solid curves) and only SO_2 is abundant (dotted curves) at FSC=0% (*a*) and FSC=0.04% (*b*).

At the mediate fuel sulfur content (FSC=0.04%) the concentration of sulfate aerosol particles with d ≥ 5 nm stays below 10^4 cm^{-3} at a distance of 1000 m from nozzle exit, and remains so even when SO_3, HSO_3, and H_2SO_4 are produced in the engine. If only SO_2 is abundant at the nozzle exit, the concentration of such aerosols is negligible. Schöder et al. measured concentration of about 10^6 cm^{-3} of relatively large volatile particles with d > 5 nm in the near field plume of the ATTAS aircraft for FSC=0.026 % [41]. These results could not be explained by the formation of sulfate aerosol precursors (SO_3, HSO_3, H_2SO_4) in the combustor.

The second idea is connected with emitted condensable hydrocarbons and CIs, which were considered to be responsible for the generation of the observed large volatile aerosols in the aircraft plume [9]. In these study the unified mechanism to form volatile particles is supposed to be coagulation between charged clusters. The key questions in this theory are following: what sorts of ions may be generated and what amount of these ions may be abundant at the nozzle exit. In order to explain measurements [41] the concentration of ions at the engine exit should be as large as $2 \cdot 10^9$ cm^{-3}. However, this value of ion concentration is believed to be too large and is not produced in modern aero-engines.

In-situ flight measurements exhibited the existence of volatile sulfate aerosol particles with d=2-5 nm at 15-20 m distance from nozzle exit. However, the Q1D models predict the formation of sulfate aerosols in the plume axis at 35-40 m distance. The appearance of sulfate particles at the short distance from engine

exit is caused by the turbulent diffusion of aerosol particles from the boundary streamline ($\bar{r}$=1) dividing the engine core flow and bypass flow to the axis of the plume. Fig.10 shows the location of the nucleation region in the plume of *B*-747 aircraft at cruise predicted by two-dimensional 2D model for turbulent plume of bypass engine.

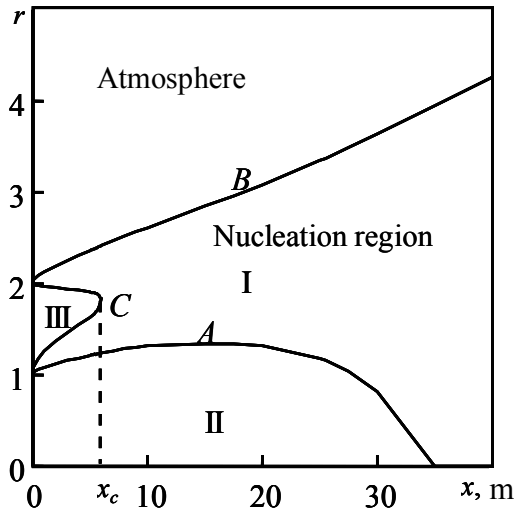

Fig. 10. Location of nucleation region in the plume of *B*-747 aircraft at cruise for FSC=0.04 % predicted by 2D model ($\bar{r}$ is the normalized radius of the plume, *A* depicts the boundary of the engine core flow, *B* depicts the boundary of the plume)

The amount of volatile aerosol particles depends on the fuel sulfur content, type of combustor, parameters at the combustor inlet, engine design, and flight altitude. Figure 11 presented by *Schumann et al.* [37] shows the variation of sulfate aerosol particle emission index PEI (PEI defined as the number of aerosol particles forming due to burning of 1 kg fuel) for different subsonic aircrafts (engines) as a function of FSC measured in-situ during a various European campaigns (Sulfur 5,6,7; SNIF; SUCCESS; POLINAT).

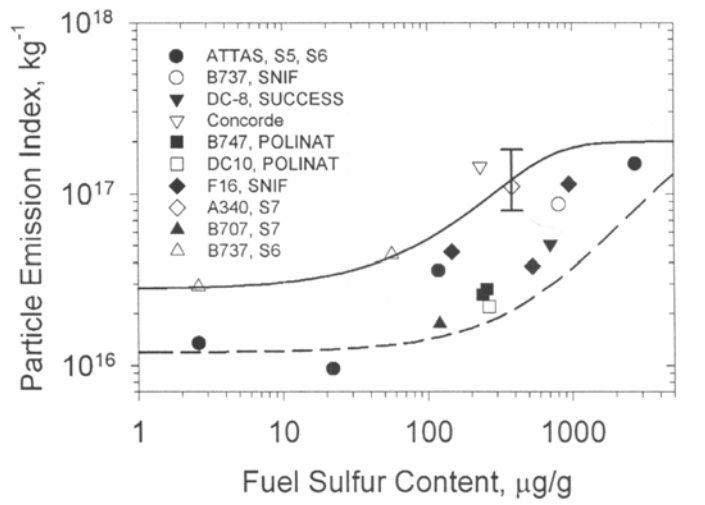

Fig. 11. Particle number emission index (PEI) of detectable volatile particles in noncontrail plumes versus FSC from various measurements normalized to plume age 3s.

Aerosol microphysical and chemical processes are similar in subsonic and supersonic aircraft plumes. The aerosol changes will differ because soot emission levels, aerosol formation potential, and plume dilution properties vary with engine type and atmospheric conditions at cruise altitudes. Significant increases in stratospheric aerosol are expected for the operation of a large fleet of supersonic aircraft, at least for non-volcanic periods.

As was mentioned above, soot particles emitted from engine consist of two fractions. One of them, the fraction of impurities, has hydrophilic properties and involves the activated particles. The second one is the main fraction and involves non-activated hydrophobic particles. These particles may be partly activated due to a deposition of solvable material on their surfaces in the plume. The simulation exhibited that general mechanisms responsible for such a process are the coagulation of soot particles with volatile sulfate aerosols and heterogeneous binary (H_2O/H_2SO_4) nucleation [30, 43]. It turned out that small size particles with diameter $d \leq 15$ nm are activated, generally, due to coagulation process and larger particles ($d > 15$ nm) are activated due to heterogeneous nucleation [30]. Depending on FSC, 5-15 % amount of soot particles of hydrophobic fraction may be activated in the plume. The activation degree grows with the FSC increase.

The other pathway of soot particle activation deals with the existence of charged soot particles in the plume. The computations show that various ionic clusters, mainly $HSO_4^-(H_2SO_4)_m$, $HSO_4^-(HNO_3)_{m-1}$ (m=1…3), $H_3O^+(CH_2O)(H_2O)_m$, and $H_3O^+(H_2O)_n$ (n=1–6) form in the plume. Their concentration at 10 m distance from engine exit may be as large as 10^6–10^7 cm^{-3} [30]. Due to dilution of the plume and attachment of ionic clusters to soot particles their concentration decreases rapidly with the plume age increase and at 50 m distance drops to 10^4–10^5 cm^{-3} that is consistent with measurements [35]. Nevertheless, the significant charge continues to be on the particle surface even to 100 m distance from the engine exit. Heterogeneous binary H_2O/H_2SO_4 nucleation on the surface of charged soot particles occurs much faster than on the neutral one.

Coated by water solution soot particles at atmospheric supersaturation conditions can condense a significant amount of water vapor that leads to an increase of their size. This is illustrated by Fig. 12 and Fig. 13, which depict the evolution of the radius of soot particles and concentration of sulfuric acid in particles the solution coating soot particles along the plume of *B-747* aircraft for particles with different initial radii (R_0) at lognormal distribution of fresh soot particles.

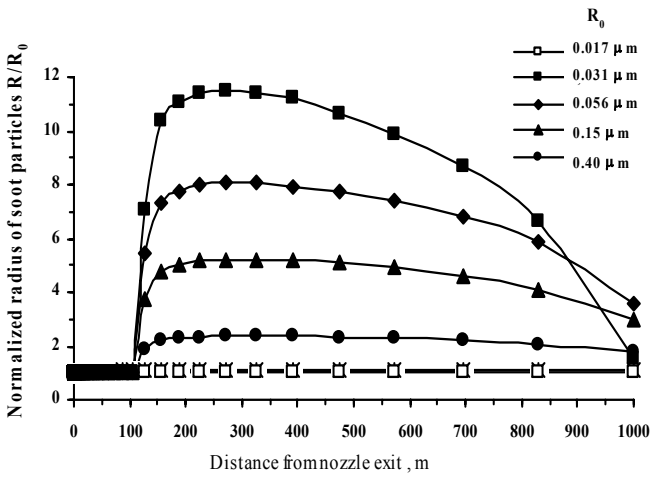

Fig. 12. Evolution of normalized soot particle radius along the plume of *B-747* aircraft at cruise for different initial radius values of fresh soot particles, R_0.

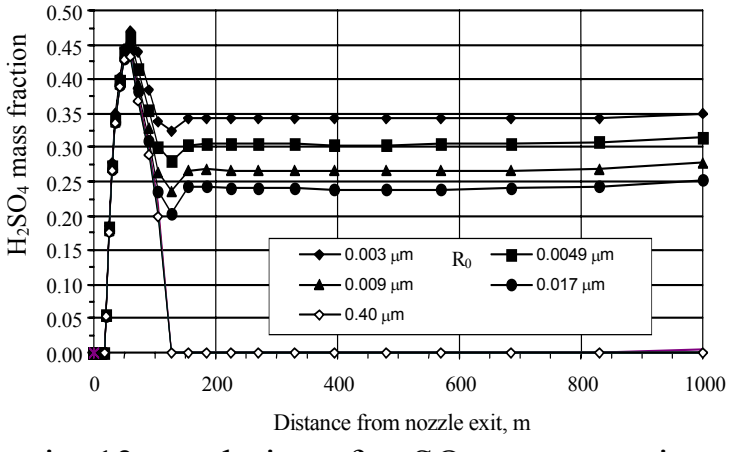

Fig. 13. Evolution of H_2SO_4 concentration in the solution accumulated on the surface of soot particles with different initial radii, R_0, along the plume of *B-747* aircraft at cruise.

One can see that only relatively large soot particles can accumulate a significant amount of water molecules on their surface. The concentration of H_2SO_4 in the H_2SO_4/H_2O solution is smaller than 10% only for particle with R_0>25-30 nm. Therefore, only these large particles can freeze. That is why the amount of ice particles observed in the plume ($N_{ice} \approx 10^3$-10^4 cm^{-3}) is significantly smaller than the number density of fresh soot particles emitted by engine ($N_s \approx 10^5$-10^6 cm^{-3}) [37].

Soot emissions for current aircraft engines are specified under the International Civil Aviation Organization (ICAO) using smoke number measurements. The smoke number is dominated by the largest soot particles collected onto a filter. Sampling soot particles smaller than about 300 nm on such filters becomes inefficient. Correlations between smoke number and soot mass concentrations may be used to estimate the soot mass EI from ICAO certification data. A mean value has been estimated to be approximately 0.04 g/(kg fuel) for the present subsonic fleet. Soot emissions depend strongly on engine types, power settings, and flight levels, additional information is generally needed to relate smoke number to emissions under flight conditions.

The diameter of soot particles emitted by aircraft engines are in the 10 nm – 100 nm range and the values of particle emission index depending on the engine type for subsonic transport aircraft vary from $1.8 \cdot 10^{14}$ - $3 \cdot 10^{15}$ kg^{-1} [37]. The soot mass (EI_{soot}) and number emission indices (PEI_{soot}) at cruise for different fleet and smoke numbers (SN) were reported by Schumann et al. [37] and are presented in Table 4.

Table 4. Soot Mass and Number Emission Indices at Cruise and Smoke Numbers[a]

Aircraft	EI_{soot}, g kg^{-1}	PEI_{soot}, 10^{15} kg^{-1}	SN at 100%	SN at 30%
B707	0.5±0.1	1.7±0.3	54.5	n.a.
ATTAS	0.1±0.02	1.7±0.35	46.3	10.9
A310	0.019±0.01	0.6±0.12	5.8	n.a.
B737	0.011±0.005	0.35±0.07	4	2.5
B747		0.27, 0.45	16.0	n.a.
DC10		0.46	11.4	1.6
A340	0.1±0.003	0.18±0.05	12.6	1.0

[a]EI_{soot} and PEI_{soot}: soot mass and number emission indices per unit mass of fuel burned; smoke number (SN) at two power settings: 100% and 30%.

Thus, besides gaseous species such as H_2O, CO_2, NO, NO_2, SO_2, SO_3, CO, and HNO_2, HNO_3, OH, N_2O in a trace amount, aircraft plume is the source of small volatile sulfate aerosol particles, neutral and charged soot particles, which may be partly activated as CCN, as well as ice particles at the conditions of contrail formation (H_2O vapour supersaturation over the water surface is necessary to form a contrail).

AIRCRAFT ENGINE EMISSIONS AND ATMOSPHERIC PROCESSES

As is believed the most important gaseous pollutants impact on the ozone concentration in the atmosphere are NO, NO_2, H_2O. Modeling studies showed that emissions of NO_x by aircraft into the stratosphere may result in ozone depletion. In contrast, the NO_x emissions into the troposphere lead to an increase of ozone concentration [2]. The quality of the effect of NO_x emissions on the atmospheric ozone depends on the surface area of sulfate stratospheric aerosol layer and polar stratospheric clouds.

In the published in 1998 paper [44] four independently formulated two-dimensional chemical transport models with sulfate aerosol microphysics are used to evaluate the possible effects of sulfur emissions from supersonic high-speed civil transport aircraft (HSCT) operating in the stratosphere in 2015. The aircraft emission scenarios employed in the estimations represented 500 aircrafts operating in the year 2015 and burning 82×10^9 kg of fuel annually, with the geographical fuel use distribution derived in [45]. The HSCT aircraft cruise at Mach 2.4, which a cruise altitude of 18-21 km. Engine emissions are specified by an emission index. The results were presented for two values of $EINO_x$, 5 and 15 g/kg. An $EINO_x$ of 5 g/kg represents a significant reduction in emission index from current supersonic aircraft (values of about 12-20 g/kg are typical), though technological advances in the last several years have shown that an $EINO_x$ of 5 g/kg is achievable. EIH_2O of 1230 g/kg is used in all calculations. The $EISO_2$ was taken to be 0.4 g/kg, based on projections that sulfur content in jet fuel will decline from its current average value of 0.8 g/kg.

All models have shown much larger increases in aerosol surface area when aircraft sulfur was assumed to be emitted as particles of 10 nm diameter rather than as gas phase SO_2. If it was assumed an emission index for SO_2 of 0.4 g (kg fuel burned)$^{-1}$ in 2015, maximum increases in stratospheric sulfate aerosol surface area range from 0.1 $\mu m^2 cm^{-3}$ to 0.5 $\mu m^2 cm^{-3}$ with sulfur emitted as SO_2 gas and from 1.0 $\mu m^2 cm^{-3}$ to 2.5 $\mu m^2 cm^{-3}$ with sulfur emitted as particles. Model differences in calculated surface area were deemed to be due mainly to differences in model transport. Calculated annual average ozone perturbations due to aircraft emissions with $EINO_x$=5 g/kg, EIH_2O=1230 g/kg, and $EISO_2$=0.4 g/kg varied from -0.1% to 0.6% at 45°N for sulfur emission as SO_2 gas and from -0.4% to -1.5% with sulfur emission as 100% particles. The variation in the ozone concentration due to HSCT emissions of SO_2 and sulfate particles of 10 nm diameter predicted by Atmospheric and Environment Research (AER) 2D model [44] is shown in Figure 14.

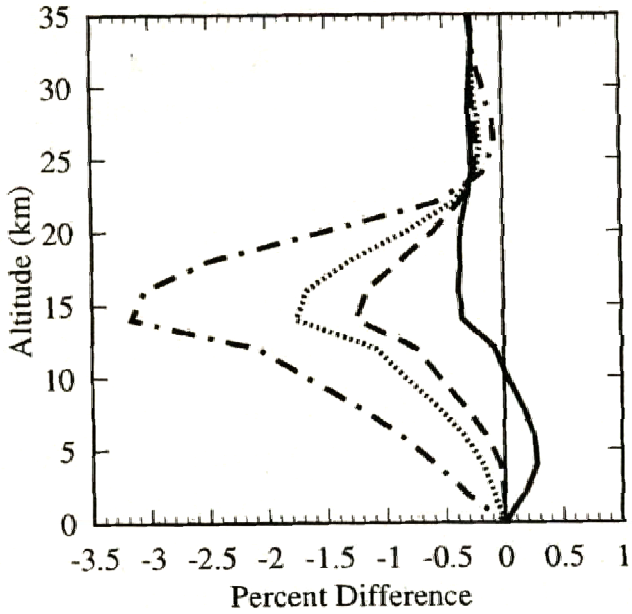

Fig. 14. Calculated percent change in the ozone concentration depending on the altitude due to HSCT emissions with a scenario: 500 aircrafts operate at cruise (M=2, H=18 km), $EINO_x$=5 g/kg, EIH_2O=1230 g/kg, $EISO_2$=0.4 g/kg, [Cl_y]=3 ppbv. The solid line represents a case with no SO_2 emissions, the dashed line represents a case with SO_2 gas emissions only, the dotted line represents a case with emissions 90% as SO_2 gas and emitted as 10%. Sulfate aerosols (d=10 nm), dot-dashed line represents a case with emissions of 100% sulfate aerosol particles (d=10 nm).

The authors of this paper strongly recommended for future analysis of HSCT impact on ozone to take into account in assessment calculations, the chemical and microphysical processes within the plume and far wake for accurate atmospheric modeling. IPCC (1999) pointed out that the future aerosol impact will depend on trends in fuel consumption, fuel sulfur content, engine soot emissions, and the efficiency with which fuel sulfur is transformed into aerosols behind the aircraft. Any aerosol increase will be enhanced if future air traffic operates at higher altitudes, because of longer atmospheric residence times of the emission products. Any climate change causing reduced temperature and increased humidity at flight levels would enhance aerosol and contrail formation.

Thus, the emissions of sulfate aerosol particles by aircrafts can significantly influence on the surface area of stratospheric aerosol layer and as a result on the radiative forcing as well as on the total ozone concentration. This exhibits the necessity of reasonable limitation on sulfate aerosol particles emitted. For modern aviation fuels the typical value of FSC does not exceed 400 μg or 0.04%. Therefore, we can suggest for prospective jet engines the limitation standard for sulfate aerosol particle emission index of (1-2)·10^{16} kg^{-1}.

The main source of carbon-containing particles in the atmosphere is the combustion of natural fuel and biomasses on the Earth's surface. Every year, up to 12 Tg of soot are emitted to the atmosphere [2]. The estimated value of soot emissions by aircraft for the year of 1992 is several orders of magnitude smaller 10^{-3} Tg. However, the role of surface sources at a height of 10 km may be insignificant because of a high activity of soot aerosols as CCN, their precipitation and washing from the lower troposphere. On the other hand, a constant increase in the frequency of aircraft flights gives grounds to predict an increase in the mass concentration of aviation soot aerosols exactly at a height of 10 km in northern latitudes. At the specified index of soot emission 0.04 g/kg, in the middle latitudes of the Northern Hemisphere, the annual maximum increase in the mass concentration of soot particles can reach 0.6 ng/m^3 [2].

According to the ICAO data, by 2050, a five-tenfold increase in the intensity of commercial flights is expected [2]. During the accumulation of soot particles in the troposphere owing to an increase in fuel consumption by aviation, the region covered with contrails is also increased. According to the prognosis given in [46], this region will be increased from 0.06 (1992) to 0.23% (2050), and, accordingly, the radiation effect of contrails will be increased by a factor of four (from 3.5 mW/m^2 to 14.8 mW/m^2). Unfortunately, the radiation effect of cirrus clouds initiated by aviation still remains to be estimated [2]. Even the sign of this effect has not been determined yet. However, it is clear that soot particles, unlike sulfate aerosols, can cause heating that leads to the cooling of the vertical temperature profile in the atmosphere, the slowing down of evaporation, and, correspondingly, to a decrease in cloud formation. Therefore, additional studies are necessary to estimate the effect of soot emissions by aviation on cloud formation and precipitation and to estimate the dependence of this effect on the physicochemical properties of aviation soot aerosols. Nevertheless, it is believed that in order to minimize the impact of aircraft flights on the atmosphere and especially on climate the limitation standard should be introduced for the soot particle emissions from prospective aircraft engines.

REFERENCES

[1] D.J. Wuebbles, A. Jain, J. Edmonds, D. Harvey, K. Hayhoe, Global change: state of the science. Environmental Pollution. 1999, 100, 57-86.

[2] D. W. Fahey, U. Schumann, S. Ackerman, P. Artaxo, O. Boucher, M. Y. Danilin, B. Kärcher, P. Minnis, T. Nakajima and O. B. Toon, in Aviation and the Global Atmosphere, A Special Report of IPCC (Intergovernmental Panel on Climate Change), ed. J. E. Penner, D. H. Lister, D. J. Griggs, D. J. Dokken and M. McFarland, Cambridge University Press, Cambridge, UK. 1999, 65–120.

[3] U. Lochman, J. Feitcher Atmos. Chem. Phys. 2005, 5, 715–737.

[4] R.P. Lindstedt and L.Q. Maurice A detailed chemical kinetic model for aviation fuels. J. Propulsion and Power. 2000, 16, 187-195.

[5] L.Q. Maurice, Detailed chemical kinetic model for aviation fuels, Ph. D. Thesis, Univ. Of London, Imperical College, Mechanical Engineering Dept., London, England, UK, 1996.

[6] C. Doute, J.-L. Delfan, R. Akrieh, and Vocell, Comb. Sci. Technol. 1995, 106, 327-341.

[7] A.M. Starik, A.M. Savel'ev, N.S. Titova, and U. Schumann, Aerosp. Sci. Technol. 2002, 6, 63-81.

[8] U. Schumann, J. Ström, R. Busen, et al., J. Geophys. Res. 1996, 101, 6853-6899.

[9] B. Kärcher, F. Yu, F.P. Schröder, and R.P. Turco, Geophys. Res. Lett. 1998, 25, 2793-2796.

[10] S.P. Lukachko, I.A. Waitz, R.C. Miake-Lye et al., J. Geophys. Res. 1998, 103, 16159-16174.

[11] A.M. Savel'ev, and A.M. Starik, Fluid Dynamics. 2001, 36, 95-103.

[12] P. Schulte, H. Schlager, H. Ziereis, et al., J. Geophys. Res. 1997, 102, 21431-21442.

[13] U. Schumann, H. Schlager, F. Arnold et al., J. Geophys. Res. 2000, 105, 3605-3631.

[14] A.B. Lebedev, A.N. Secundov, A.M. Starik, S.A. Schepin, N.S. Titova In Nonequilibrium processes: Combustion and Detonation. Ed. G.D. Roy, S.M. Frolov, A.M. Starik. Moscow. Torus Press Ltd. 2005, 1, 158-167.

[15] Prather M.J., Wesoky H.L., R.C. Miake-Lye and et al. The Atmospheric Effects of Stratospheric Aircraft:A First Program Report. NASA Reference Publication 1272. 1992.

[16] G.P. Smith, D.M. Golden, M. Frenklach, N.W. Moriarty, B. Eiteneer, M. Goldenberg, C.T. Bowman, R.K. Hanson, S. Song, W.C. Gardiner, V.V. Lissianski, Z. Qin http://www.me.berkley.edu/gri_mech/

[17] A.A. Konnov Detailed reaction mechanism for small hydrocarbons combustion. 1998. Release 0.4 http://homepages.vub.ac.be/~akonnov.

[18] N.G. Dautov and A.M. Starik, Kinetics and Catalysis. 1997, 38, 185-208.

[19] A.B. Fialkov, Prog. Energy Combust. Science. 1997, 23, 339-528.

[20] F. Yu, R.P. Turco, J. Geophys. Res. 1998, 103, 25.915-25.934.

[21] A.M. Savel'ev and A.M. Starik, Tech. Phys. 2006, 51, 444-452.

[22] P. Weilmuster, A. Keller, K.H. Homan, Combust. Flame. 1999, 116, 62-83.

[23] A. Kiendler, St. Aberle, F. Arnold, Atmos. Environ. 2000, 34, 2623-2632.

[24] J.M. Rodrigues, A. Agneray, X. Jaffrézic et al. Plasma Sources Sci. Technol. 2007, 16, 161-172.

[25] H. Haverkamp, S. Wilhelm, A. Sorokin, and F. Arnold. Atmos. Environ., 2004, 38, 2879-2884.

[26] N. Peters. Turbulent Combustion, N.-Y.: Cambridge University Press. 2000.

[27] A.M. Starik, A.M. Savel'ev and N.S. Titova Proceedings of Second International Workshop on Cold Atmospheric Pressure Plasmas: Sources and Applications. Bruges, Ghent University. 2005, 118-122.

[28] Soot Formation in Combustion: Mechanisms and Models, Ed. by H. Bockhrom. Springer, Berlin. 1994.

[29] D.D. Huang, J.H. Seinfeild, and K. Okuyama. J. Colloid and Interface Science. 1991, 141, 191-198.

[30] A.M. Starik, O.B. Popovicheva, A.M. Savel'ev, N.S. Titova, O.E. Reyn Chemical Engineering Transaction. Proceedings of Advanced Atmospheric Aerosol Symposium. Ed. by E. Ranzi. 2006, 10, 541-546.

[31] O.B. Popovicheva, N.M. Persiantseva, E.E. Loukhovitskaya et al. Geoph. Res. Lett. 2004, 31, L11104, doi: 10.1029/2003GL018888.

[32] A.M. Starik, A.M. Savel'ev, N.S. Titova, O.E. Reyn. In Combustion and Atmospheric Pollution. Ed. by G.D. Roy, S.M. Frolov, A.M. Starik, Moscow Torus Press. 2003, 470-473.

[33] S. Böckle, S. Einecke, F. Hildenbrand et al. Geophys. Res. Lett. 1999, 26, 1849-1852.

[34] U. Schumann, H. Schlager, F. Arnold et al. J. Geophys. Res. 2000, 105, 3605-3631.

[35] F. Arnold, K.H. Wohlfrom, M.W. Klemm et al. Geophys. Res. Lett. 1998, 25, 2137-2140.

[36] A. Kiendler and F. Arnold, Atmosph. Environment. 2002, 36, 2979-2984.

[37] U. Schumann, F. Arnold, R. Busen et al. J. Geophys. Res. 2002, 107, 10.1029/2001JD000813.

[38] A.M. Starik, A.M. Savel'ev, N.S. Titova, E.E. Loukhovitskaya, and U. Schumann. Phys. Chem. Chem. Phys. 2004, 6, 3426-3436.

[39] A. Petzold, A. Dopelheuer, C. Brock, F. Schroder. J. Geophys. Res. 1999, 104, 22171–22181.

[40] R.C. Brown, R.C. Miake-Lye, M.R. Anderson, C.E. Kolb. Geoph. Res. Lett. 1996, 23, 3607-3610.

[41] F.P. Schröder, B. Kärcher, A. Petzold et al. Geoph. Res. Lett. 1998, 25, 2789-2792.

[42] F. Arnold, K.H. Wohlfrom, M.W. Klemm, J. Schneider, K. Gollinger, U. Schumann and R. Busen. Geophys. Res. Lett. 1998, 25, 2137.

[43] N.K. Shonija, O.B. Popovicheva, N.M. Persiantseva, A.M. Savel'ev, and A.M. Starik. J. Geophys. Res. 2007, 112, D02208, doi:10.1029/2006JD007217.

[44] D.K. Weisenstein, M.K.W. Ko, I.G. Dyominov et al. J. Geophys. Res. 1998, 103, 1527–1547.

[45] S.L. Baughcum, S.C. Henderson Aircraft emission scenarios projected in year 2015 for the NASA technology concept aircraft (TCA) high speed civil transport. NASA/CR-1988-207635, National Aeronautics and Space Administration, Hampton, VA, 1998. 21 p.

[46] S. Marquart, M. Ponater, F. Marger, and R. Sausen. "Future Development of Contrails: Impact of Increasing Air Traffic and Climate Change" in Air Pollution Report No.83 "Aviation, Atmosphere, and Climate" EC, 2003, 255-260.